Advanced Powder Technology 34 (2023) 103950

Contents lists available at ScienceDirect

Advanced Powder Technology

journal homepage: www.elsevier.com/locate/apt

Characterising the sedimentation of bidisperse colloidal silica using analytical centrifugation

Hangyu Chen *, Xiaodong Jia, Michael Fairweather, Timothy N. Hunter *

University of Leeds, School of Chemical and Process Engineering, Leeds LS2 9JT, UK

ARTICLE INFO

Article history:
Received 15 September 2021
Received in revised form 17 January 2022
Accepted 10 January 2023

Keywords:
Bidisperse colloids
Bidisperse sedimentation
Batchelor model
Backflow

ABSTRACT

This study investigates the settling behaviour of bidisperse colloidal silica suspensions in two different size ratios (100:500 nm and 500:800 nm) with various mixture ratios and volume fractions, using an analytical photocentrifuge. For dilute systems, translation of settling rate profiles to size distributions resulted in more accurate measurements for both monodisperse and bidisperse systems than using dynamic light scattering, in comparison to SEM. However, a critical limitation was also observed, as distinction between upper (smaller particle) and lower (larger particle) interfaces could only be measured for total volume fractions <~0.02. For 500:800 mixtures, results were compared with Richardson-Zaki and modified Batchelor model predictions. The Batchelor model proved more accurate at predicting the lower interface rate, while both models over predicted the upper interface, likely due to increased drag that was most evident with higher fractions of smaller particles. For 100:500 cases, higher centrifugal rotation speeds were required to settle the 100 nm particles, and the influence of Brownian motion was evident. It was also found that the smaller particles obtained a lower initial settling rate than its terminal velocity, due to induced anisotropic effects or backflow from the 500 nm fraction, which was again more evident with a greater proportion of smaller particles.

1. Introduction

The sedimentation of colloidal suspensions has been intensively studied for many years [1–3]. Its importance is found in many practical applications, such as solid–fluid separations [4–6], food [7], as well as cosmetics and paints [8], where sedimentation theory is used to predict the efficiency of industrial processes or product shelf-life, for example. Therefore, a number of studies have been reported over the years on characterising complex colloidal settling (e.g., [9,10]) and the prediction of settling rates (e.g., [11,12]). The Richardson-Zaki model [13] is one of the most popular methods to predict changes to sedimentation with concentration, using an empirical power-law hindrance function. Alternatively, Bachelor [14] derived a linear relationship between the mean fall velocity of a particle and the concentration for diluted monodisperse suspensions, where the coefficient of the equation has been further discussed and modified by other authors (e.g., [15,16]). These two models are in relatively good agreement for semi-dilute and dilute suspensions [17]. Related models that are suitable for higher particle concentrations [18] and larger particle ranges [19] have also been proposed.

In addition to empirical models, there are also mathematical treatments of sedimentation which relate the settling velocities to the properties of suspensions. In particular, Kynch's one-dimensional monodisperse zonal sedimentation model [20] is regarded as the first truly numerical model for the sedimentation and separation of particle fractions forming incompressible cakes. It has been further extended by various authors (e.g., Davis and Russel [21] who included Brownian diffusion for colloidal particles, and van Deventer *et al.*, who incorporated aggregate densification [22]). While these numerical models have been used to predict the hindered settling velocity of various systems [23], they are relatively mathematically intensive, and are most suited to studies focused on the compressive consolidation of dispersions rather than dilute or semi-dilute settling.

Peer review under responsibility of The copyright line should read:002: Copyright © 2014, The Society of Powder Technology Japan. Published by Elsevier BV and The Society of Powder Technology Japan. All rights reserved.001: Copyright © 2014 Published by Elsevier B.V. on behalf of The Society of Powder Technology Japan. All rights reserved.Please add this footnote for the item group IG000042 "This is the article featuring on ICBMH2019: the 13th International Conference on Bulk Materials Storage, Handling and Transportation."

* Corresponding authors.
E-mail addresses: pmhch@leeds.ac.uk (H. Chen), t.n.hunter@leeds.ac.uk (T.N. Hunter).

https://doi.org/10.1016/j.apt.2023.103950
0921-8831/

For real industrial processes and products, one of the greatest challenges in predicting sedimentation and separation is that systems are not always monodisperse, and in fact, bidisperse and polydisperse suspensions are more common. Bidisperse suspensions can be regarded in many ways as the 'simplest' case of polydisperse systems, allowing investigations into the underlying mechanisms of multi-sized particle settling. For example, Richardson and Zaki [24] proposed a modification based on monodisperse suspensions for application to polydisperse systems, using the total volume fraction of particles. Other investigations have showed, nonetheless, that this formula did not match well with experiments of large differences in size or density [25], although further modification to power-law models for sedimentation of bidisperse and polydisperse dispersions have been proposed [26,27]. Also, empirical models have not always proved to be accurate in bidisperse sedimentation, especially for large particles [28]. While the sedimentation of polydisperse systems is more complex than bidisperse, it is known to be strongly influenced by the size distribution of particles [29]. Therefore, the use of multiple particle size ratios in investigations will aid in understanding the interaction between different size classes. It has also been reported that the mixing ratio of particles influences the relative viscosity of species in bidisperse sedimentation [30], which is not something that is fully taken account of in most analytical sedimentation models.

Another complexity with studying fine colloidal systems is that separation occurs naturally over extended periods of time that is difficult to measure accurately, and may be subject to other forces such as Brownian motion [10], which counters the gravitational movement. To overcome challenges of slow settling systems, centrifugal sedimentation is a simple but useful intensified solid–liquid separation method. Within the high value chemicals industry, centrifugal separators are a very common method to accelerate settling processes; either for solids waste management [31–33] or as an investigative technique to study products which are formulated for long shelf lives [34–36]. In particular, laser based centrifugal analysers can simultaneously track interfacial settling rates of multicomponent systems, using scanning light transmission data. Modern instruments have been developed into very useful tools to investigate colloidal suspensions, allowing illumination across their entirety by having detectors that can measure light extinction profiles instantaneously with micrometre scale resolution [37].

It is reported that even very small changes in dispersion state can be detected. For example, Lerche [38] characterised both mono and polydisperse systems ranging from nano to micro sized with the same instrumentation, showing the high reliability of centrifuge data and analysis methods. Analytical centrifuges can also measure the size distribution of suspensions, where results have been shown to be more accurate than dynamic light scattering (DLS) devices [39] especially for bidisperse and polydisperse nanoparticles [40], and have been used to separate bidisperse charged nanoparticle suspensions [41]. Furthermore, centrifugal sedimentation may lead to enhanced Reynolds number dependent wake effects [42], as well as Drafting-Kissing-Tumbling (DKT) events [43,44] that can lead to a modified drag force acting on trailing particles. This phenomena has been verified by simulations [42] and has been found to be even more prevalent in dilute suspensions [45].

While significant theoretical and experimental work exists on bidisperse settling, as outlined, considerable questions remain into their sedimentation dynamics and, in particular, the interactions between one size fraction on the settling of another. Especially for fine colloidal systems, more understanding is required into the effect of size and concentration ratios on sedimentation, and whether changes in specific ratios significantly affect particle drag or enhance wake effects. Such changes may also modify the accuracy of common sedimentation models that are widely used industrially for predicting behaviour. Additionally, while it is clear analytical centrifugation has become a standard technique for characterising slow-settling dispersions over the last decade or so, analysis of multi-species systems is still complex. Limitations exist from the interaction of particle species on total light transmission of particle fractions, which needs to be clearly defined for bidisperse systems.

Therefore, the aim of this work is to investigate the sedimentation of bidisperse colloidal particles of the same material with an analytical centrifuge. Specifically, two size particle ratios of colloidal silica are used (500:800 nm and 100:500 nm sizes) in various mixing ratios and total volume fractions. Sedimentation profiles from dilute systems are converted to size distributions and compared to dynamic light scattering and scanning electron microscopy (SEM) for comparison. Then, the fractional interfacial sedimentation rates are measured for various systems, where instrumental limitations due to reduced light transmission are examined. Extracted settling rates of both the larger and smaller particle fractions are then compared to bidisperse modified Richardson-Saki and Batchelor models. These are used to highlight the influence of mixture ratios on particle drag or wake effects that may alter the following object's velocity from local hydrodynamic interactions.

2. Materials and methods

2.1. Materials

The colloidal silica particles used were Angstrom Sphere® silica powder, with nominal quoted mean sizes of 100, 500 and 800 nm (Fiber Optic Center Inc., USA). The particle densities (ρ_p) were measured as 2.2 g/cm^3 for the 100 nm silica particles and 1.92 g/cm^3 for the 500 nm and 800 nm particles, using a Pycnomatic ATC gas pycnometer (Thermo Electron, USA). The density results are close to expectations for silica particles [46]. Suspensions were prepared by adding silica powder to a 1×10^{-4} M potassium chloride (KCl) background electrolyte solution, using KCl crystalline powder (Fluka Chemie GmbH, Germany) and ultrapure Milli-Q™ water, with a resistivity of 18.2 MΩ.cm at 298 K (Millipore, USA). The suspensions were placed in an ultrasonic bath (XUBA3, Grant) for 15 min prior to characterisation without heating. Samples were then further dispersed using an ultrasonic Sonic Dismembrator (Fisher Scientific) at 80% amplitude for 5 min. The purpose of the ultrasonic bath and probe was to fully homogenise the suspensions before any measurements were taken.

Two different size ratios were investigated, comprising nominal 500 and 800 nm silica particles (with a relative mean size ratio of 1.6) as well as 100 and 500 nm particles (with relative mean size ratio of 5). Bidisperse nanoparticle suspensions (500: 800 nm and 100:500 nm) were prepared in three relative mixing ratios on a volume basis (1:2, 1:1, 2:1). The total volume fractions of the bidisperse suspensions ranged from 0.001 to 0.03 for the mixture of 100 nm and 500 nm particles, and from 0.0005 to 0.05 for the mixture of 500 nm and 800 nm particles. It is noted that while the actual particle size distributions were confirmed through detailed characterisation (see Section 2.2) for simplicity, the species are labelled as per the manufacturer specifications throughout (100, 500 and 800 nm sizes).

2.2. Particle characterisation

A Zetasizer® Nano ZS dynamic light scattering analyser (Malvern Panalytical ltd., UK) was used to confirm the size distribution of the silica particles. Dispersions at 1000 ppm concentration were

firstly prepared using the procedure outlined above. For the measurements, three separate samples were analysed over a 120 s measurement time with three runs for each sample. Autocorrection functions were fitted using the Zetasizer® "general purpose mode" for the monodisperse systems and "multiple narrow modes" for the bidisperse suspensions. Additionally, ultra-high-resolution scanning electron microscopy SU8230 (Hitatchi, ltd.) was used as a further method to confirm average particle sizes and particle morphology. To enhance the electrical conductivity, dry silica particles from the manufacturer were placed as a monolayer under high vacuum conditions and coated with a layer of carbon on a standard SEM stub. Energy-dispersive X-ray spectroscopy (EDS) was also used to ensure samples were pure silica particles without any contamination.

2.3. Centrifugal sedimentation experiments

Phase separation of both monodisperse and bidisperse suspensions was monitored using a LUMiSizer® analytical centrifuge (LUM GmbH, Germany). The LUMiSizer® [38] enhances sedimentation by exposing sample dispersions to a centrifugal acceleration greater than earth gravity. The analysis uses a method called 'Space and Time resolved Extinction Profile' (STEP®) technology, which is an updated approach from classical static light scattering [37]. The centrifuge rotation rate can be altered from 0 to 4000 rpm and the effective detection zone ranges from 105 to 130 mm. In the LUMiSizer®, a light source pulses near-infrared (865 nm) light through the side of each sample cell at user-specified times. The light intensity was normalised prior to each run. A 25 mm 2048 element CCD-line detects the intensity of transmitted light across the length of the sample, yielding transmission profiles that can be converted to interface sedimentation, using appropriate transmission thresholds. The transmission profiles were recorded every 10 s throughout each run. Each sample was sealed and placed horizontally in the analyser, along the radial axis, with the top of the sample nearest to the centre of rotation. The base of sample was determined to be at a radial distance of 129.3 mm from the centre of rotation. The centrifugal acceleration, a, is given by Eq. (1):

$$a = (2\pi n)^2 r \tag{1}$$

where n is the number of centrifuge revolutions per second and r is the radial position in the centrifuge, with r = 0 at the centre of rotation. The height of sample cell in the centrifuge in this study is 20 mm. Due to the position of the sample in the centrifuge, r is given by Eq. (2):

$$r = r_{\max} - x \tag{2}$$

where r_{max} is the radial position (m) at the base of the sample and x is the position. As the particles sediment towards the end of the tube, the acceleration does slightly increase with the settling interface. For this study, it ranged from 975 m/s^2 to 1195 m/s^2 (estimated from the change in x between the start and end of each experiment). Initially, the sedimentation of monodisperse nanoparticle suspensions (nominal 100, 500 and 800 nm as detailed) were measured for volume fractions ϕ = 0.001–0.03. Then, the sedimentation of bidisperse suspensions of 500:800 and 100:500 nm mixtures were measured for total volume fractions of ϕ = 0.001–0.03, using the particle mixing ratios described in Section 2.1.

To verify some of the trends observed using the centrifugal analyser, a Turbiscan® earth gravity optical analyser was also used (Formulaction, France). Dispersions were added to 20 ml sample cells and the optical transmission and backscatter were obtained every 10 min automatically. The total measuring time was 48 h, due to the slow settling of the colloidal particles under earth gravity.

3. Results and discussion

3.1. Dispersion characterisation

Scanning electron micrograph images were obtained for the silica sphere particles, as shown in Fig. 1. From these results, particles are confirmed as spherical in morphology and close to the size provided by the manufacturer, see example particle sizing in the figure annotations. Further, size distributions derived from SEMs are shown within the Electronic Supplementary Material (ESM), Fig. S1. The average size from SEM distributions were very close to manufacturer expectations for the 500 and 800 nm particles, but were ~ 15% larger than expected for the 100 nm particles. For sedimentation analysis, the measured means were used in calculations.

As well as being used to directly analyse bidisperse sedimentation at various concentrations (see proceeding sections) the LUMiSizer® analytical centrifuge was also utilised to measure particle size distributions, based on an integration of the settling velocity and Stokes law.

Here, the extension value, E, can be transformed from transmission values and is related to the fraction of particles at a given displacement, where it is a ratio of the measured transmission of the dispersion, T, and the transmission of the sample cell filled with the dispersion media only (T_0). Then, the extension value E at a given displacement is calculated, according to Eq. (3):

$$E = -\ln\left(\frac{T}{T_0}\right) \tag{3}$$

A given particle size can be measured using the centrifuge modified Stokes law, as given in Eq. (4):

$$d = \sqrt{\frac{18\eta_f}{(\rho_p - \rho_f)\omega^2 t_m}\ln\left(\frac{r_m}{r_0}\right)} \tag{4}$$

where d is the particle diameter (m) of spherical particles in an unhindered laminar sedimentation regime. ρ_p is the particle density (kg/m^3), ρ_f is the fluid density, ω is the angular speed (radians/s), η_f is the dynamic viscosity of the fluid (Pa·s), r_0 is the starting position of the particle (m), r_m is the measurement position (m), and t_m is the measurement time (s).

The 'Constant Position' approach, which is used in particle size measurements from LUMiSizer® data, is based on the time source of the registered intensity of the emergent beam. Alternatively, the particle velocity can be determined from the 'Constant Time' approach by measuring the travelled distance of particle in a given time, t, by spatial resolving. The cumulative volume weighted particle size distribution, $Q(d)$, is calculated directly from the integration of the extension values across the profile length. The volumetric cross section, A_v, is calculated from Mie theory [47] or determined experimentally. Here, $E(r)$ is the extinction and can be used as the dependent variable, with position, r, as independent variable to calculate the distributions of velocity and size.

$$Q(d) = \frac{\int_{E_{\min}}^{E(r)} \frac{r^2}{A_V(d)}\,dE(r)}{\int_{E_{\min}}^{E_{\max}} \frac{r^2}{A_V(d)}\,dE(r)} \tag{5}$$

The cumulative volume weighted particle size distribution, $Q(d)$, can be obtained directly from the extinction profiles, which equates the volume percent (%) of undersize particles. Then, the volume weighted distribution density $qln(d)$ can be calculated,

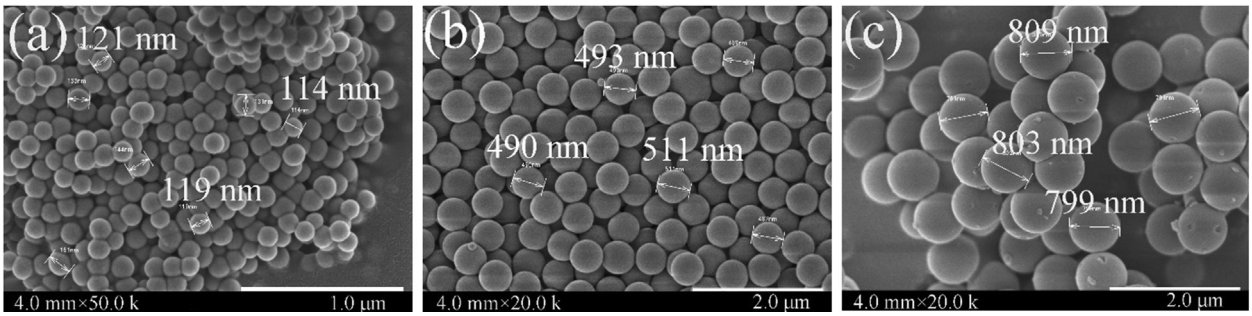

Fig. 1. Scanning electron micrographs of silica nanoparticles, with nominal mean sizes of (a) 100 nm (50.0 k magnification), (b) 500 nm (20.0 k magnification), (c) 800 nm (20.0 k magnification).

and can be regarded as qualitatively equivalent to a volume percent distribution [48], at least for the purposes of peak matching. The light transmission profiles of monodisperse systems are shown within the Electronic Supplementary Material (ESM), Fig. S2, and the resulting weighted density particle size distribution (PSD) results are shown in Fig. 2, where they are compared to volume % PSDs measured by dynamic light scattering using the Zetasizer®. It is noted that only dilute systems can be analysed using the Stokes equation to estimate size, and the data in Fig. 2 were generated from dispersion volume fractions of 0.001. For a more direct comparison, the volume % distributions from DLS were also converted to the weighted distribution, *qln(d)*, function, as given within the ESM, Fig. S3, with results being consistent with trends displayed in Fig. 2.

From the monodisperse PSD results, all three types of silica particles were measured to be close to their manufacturer defined sizes, especially for the 500 and 800 nm particles, while their polydispersity indexes from DLS were 0.031, 0.012 and 0.07 for the nominal 100, 500 and 800 nm particles respectively, confirming that the suspensions are all nearly monodisperse [49]. Interestingly, results also suggest that sizes measured from the LUMiSizer® were both closer to the manufacturer specifications, and with much smaller distributions than through DLS (which can be visually observed in Fig. 2 for all three particle types). Similar results have been found by Chiu and co-workers [39], for example, who compared size distributions of organic/inorganic coatings from analytical centrifuge and DLS, also reporting that the analytical centrifuge produced more accurate PSDs. The limitations of DLS measurements for particle size have also been discussed by Anderson *et al.* [50], who suggested that DLS is not suitable for measuring particles with broad size distributions, while they also found that the analytical centrifuge was one of the best techniques to study non-monodisperse particle systems.

The main considered reason for the distribution broadening is the relative influence of larger particles on scattered intensity (where $I \propto d^6$ in the Rayleigh regime)[51]) meaning that only a few larger particles or aggregates can skew the data or increase the error in the autocorrelation inversion [52]. While the larger 800 nm particles in this study would be strictly outside of the Rayleigh limit, the issues of peak broadening are reduced, bur remain. In this case also, the particles are towards the upper measurable limit by DLS, due to their small Brownian diffusions. Additionally, DLS measurements may be affected by any associated bound ion or electrical double layers, due to their effect on Brownian diffusion (and thus measured hydrodynamic diameter) which is most prevalent when they are of the same size order as the particles themselves [53]. In fact, it is evident from Fig. 2 that the DLS overestimates the smallest 100 nm particles more so than the 500 or 800 nm particles, where the relative double layer effects will be more significant.

Importantly, the LUMiSizer® matched the SEM estimations for the nominal 100 nm particles, with measurements giving a mean size of ~ 115–120 nm. Further, the LUMiSizer® detected a small degree of aggregation, as evident in the distribution in Fig. 2(a), which visually affected the transmission profiles to those expected from a true monodisperse system (see also Fig. S2(a)) although this did not significantly alter the mean sizes. To further probe the influence of any aggregation of the fine particles, 100 nm dispersions were also analysed at 1000 and 4000 rpm using a 0.005 vol fraction for comparison, with results presented within the ESM, Fig. S4, along with the related velocity distributions. Similar to the 0.001 vol fraction data presented in Fig. 2, there is evidence

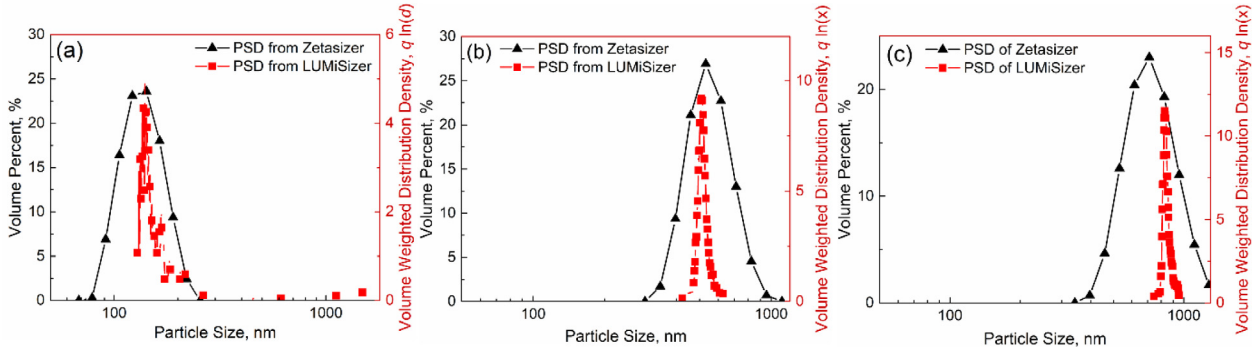

Fig. 2. Particle size distributions of the three nano-silica dispersions, as measured by the Zetasizer® as a volume distribution (black, left hand axis), and by the LUMiSizer® as a volumetric differential distribution (red, right hand axis). Particles have nominal sizes of (a) 100 nm, (b) 500 nm, and (c) 800 nm. (For interpretation of the references to colour in this figure legend, the reader is referred to the web version of this article.)

of a particle aggregation peak (which is more noticeable in terms of velocity, as related to size squared) although, again, the aggregates don't affect the detection of the primary mean.

To further investigate the comparison of analytical centrifuge and DLS, bidisperse particle size distributions of the 100:500 and 500:800 ratio systems (both at a relative volume mixing ratio of 1:1) are shown in Fig. 3. It is clear, again, that the DLS size data has a greater level of polydispersity that the centrifuge measurements. For the 500:800 mixture, the increase in the measured size range is to a level where only a broad monodisperse peak is actually measured, rather than the two discrete sizes, which are, however, clearly analysed with the centrifuge. From the LUMiSizer® distributions also, the intensities of the two peaks are relatively close in both systems, indicating that the mixing ratio of 1:1 was recovered by the weighted distribution correctly. In general, the bidisperse suspensions accentuate the trends observed in the single particle systems where the DLS technique leads to greater spread in the size measurements, which is not consistent with the level of dispersity evident with the centrifuge or SEM.

3.2. Sedimentation of 500 and 800 nm particle mixtures

An example LUMiSizer® light transmission sedimentation profile of a 500:800 nm particle mixture is presented in Fig. 4 to illustrate a typical change with time in transmission percentage over the sample height. Each profile signifies the transmission situation at a particular time, with green colours representing transmission at the end of the measurement, and a red colour designating profiles at the beginning. When there are two kinds of particles at different velocities, as in the example provided, the profile will present an inflection point that represents a border between particle factions, which can be tracked by the instrument. The transmission profiles in Fig. 4 clearly highlights two species are present at higher and lower transmission levels [54] that settle with time, with each curve representing a time period of 10 s. The higher percentage transmission represents the upper interface (smaller 500 nm silica in this case) while the lower one represents the larger 800 nm silica particles. The mean interface positions are defined and tracked using the average transmission in each fraction. As sedimentation occurs, the profiles move from the meniscus to the bed. The mean sedimentation velocities of the two particle

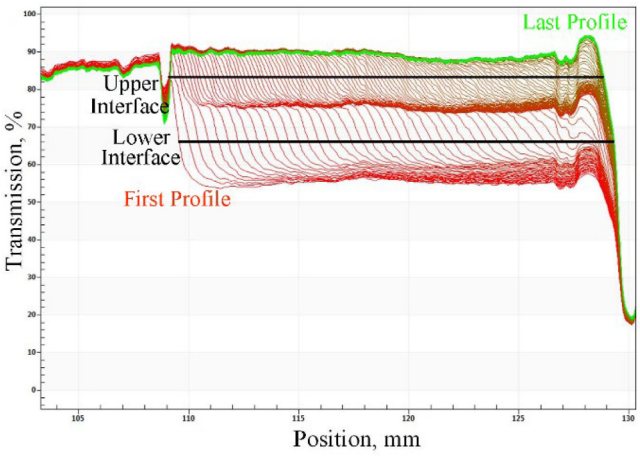

Fig. 4. LUMiSizer® transmission profiles of bidisperse silica suspensions (500 and 800 nm particles) at a volume ratio of 1:1 and total volume fraction of 0.001, under a 1000 rpm centrifuge speed. Solid horizontal lines indicate mean transmission values for each separate interface.

fractions can be determined from the change in the average interface positions (shown by the horizontal bars in Fig. 4) over time. It is clear, in the case presented in Fig. 4, that the lower interface sediments faster (and thus is associated with the larger particle species) from the greater separation between each transmission profile.

What is an important consideration in the analysis is how the total particle volume fraction of the two species affects total transmission, and thus the ability to designate each separate interface. It is also noted that the measured transmission is not strictly equal to the transmission within suspension sample. Instead, it can be considered as a normalised total transmittance, which also depends on light reflection from the sample walls. To better understand these limitations, given in Fig. 5 are the average mean transmission positions and ranges for the upper and lower interfaces at various total volume fractions of 500:800 nm mixtures, for relative volume ratios of 1:2, 1:1 and 2:1. It is clear that the transmission of the lower interface 'disappears' with an increase in the total volume fraction of the particles, a phenomenon that is slightly more

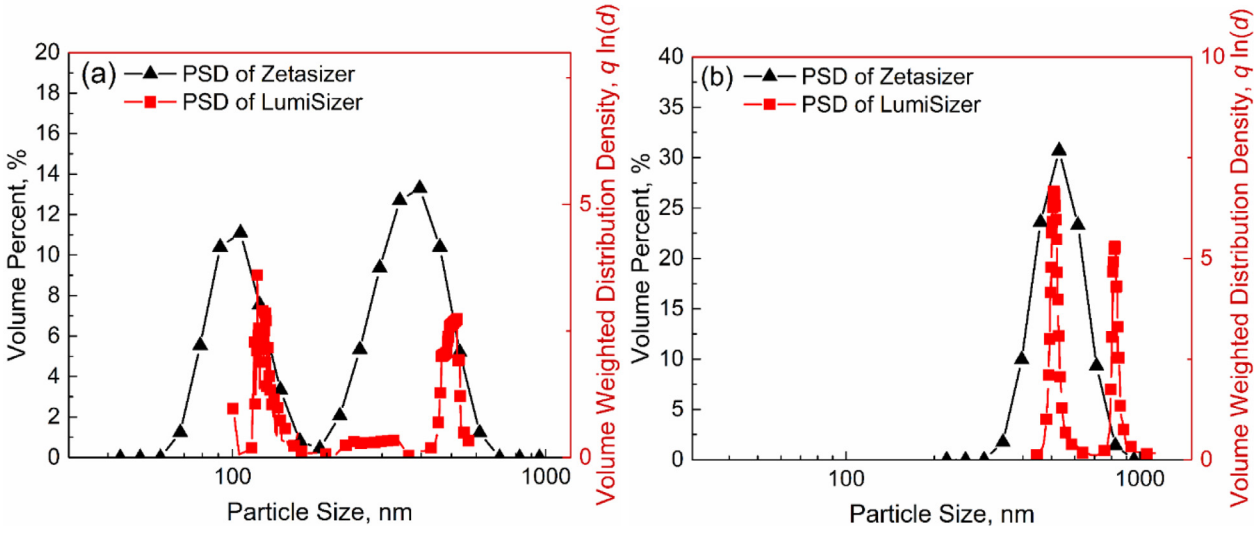

Fig. 3. Particle size distributions for bidisperse silica systems, as measured by the Zetasizer® as a volume distribution (black, left hand axis), and by the LUMiSizer®, as a volumetric differential distribution (red, right hand axis). Shown are 1:1 vol ratio dispersions for the cases of (a) 100 and 500 nm particles, and (b) 500 and 800 nm particles. (For interpretation of the references to colour in this figure legend, the reader is referred to the web version of this article.)

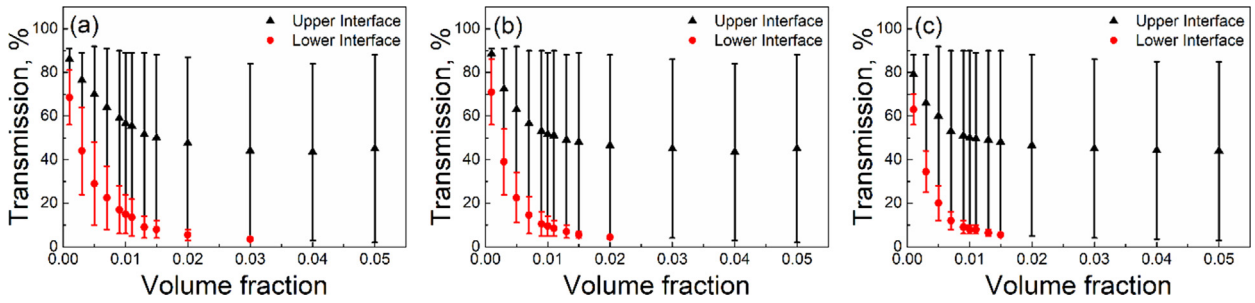

Fig. 5. Time averaged LUMiSizer® light transmission profiles for the case of 500: 800 nm particle mixtures under 1000 rpm at various total volume fractions, with different volume ratios of (a) 1:2, (b) 1:1, and (c) 2:1. Datapoints represent mean time averaged values of the interface transmission, while scale bars represent averaged transmission range of each interface.

pronounced with a higher ratio of smaller species. Essentially, the lower interface can only be detected if there is a measurable transmission difference between the 500 and 800 nm particle fractions. If the upper dispersion fraction has zero transmission (e.g., the initial concentration of the smaller particles is great enough to fully extinguish the light through the cell) then it is not possible to distinguish the lower interface, and it is masked. Therefore, there is an upper limit to the particle volume fractions that can be measured in bidisperse systems with this device. Although the lower interface of the 1:2 was recognised at 0.03, it is very hard to obtain any statistical data. From the results presented in Fig. 5, the highest concentration that two interfaces could still be clearly detected was a volume fraction of 0.02 (in the case of the 1:2 and 1:1 ratio systems) and 0.015 (for the 2:1 system).

Some samples were also characterised with the Turbiscan® gravity settling system, to confirm the reasons for the extinguishment of the lower interface in the LUMiSizer®. While the Turbiscan® does not utilise centrifugal force to accelerate phase separation, it has a backscatter detector that can be used to measure interfaces in concentrated systems that exhibit zero transmission. These results are shown within the ESM (Fig. S5) for a 1:1 ratio system of 500:800 nm particles, at total volume fractions of 0.02 and 0.04. Each interface could be tracked clearly in both cases, highlighting that size fractional separation occurs at higher concentrations, and the lack of a second visual interface with LUMiSizer® data (beyond a volume fraction of 0.02) is simply from instrument limitations. The result means that total volume fractions are still below a point where hindered settling becomes significant enough to impede size fraction separation, which would cause sedimentation to occur alternatively through a collective zonal front [12].

While there were limitations to the analysis by the LUMiSizer®, for total volume fractions ϕ = 0.02 and below, the front tracking model was clearly able to differentiate the average settling velocity of each interface for suspensions below this concentration. An example of the front tracking data is given Fig. 6, showing the normalised height versus time (for the case of total volume fractions of 0.01 and 0.015 and a 1:1 vol ratio of 500:800 nm particles at 1000 rpm). Other example datasets for the 500:800 particle systems are given within the ESM (Fig. S6).

The average settling rate for each interface can be determined from the linear gradient change (indicated by dashed lines in the figure). Clear delineation between the interfaces is observed and assumed to correlate to the separated size fractions. Additionally, it is noted that the actual experimental change in height versus time is not quite linear. The change increases slightly towards the end of the running time, with the interfaces near the base of the sample tube (which is more noticeable for the slower, upper, interface). This phenomenon is to be expected, and due to the enhancement in centrifugal force as the interface moves outwards as sedimentation continues, causing particle depletion [11]. Nonetheless, given the relatively small nature of this deviation, the average linear change in height versus time was used to estimate the mean settling rate for each particle species as concentration was varied (for tests at both 1000 and 2000 rpm). To further confirm the accuracy of the front averaging, velocity distributions for example 500:800 mixtures were extracted using the constant position mode, where the peak means were compared to estimates from front tracking (see ESM, Fig. S7 & and Table S1). Both methods gave values within 5%, although the front tracking method was used in the results presented due to its simplicity.

For the various sedimentation rate data collected, results were compared firstly to the Richardson-Zaki ('R-Z') model [24] to understand the influence of concentration on interface settling rates. The R-Z model for bidisperse systems can be described as follows in Eq. (6) and Eq. (7):

$$v_i = u_i^0 f_i \tag{6}$$

$$f_i = (1-\phi)^n \tag{7}$$

Here, v_i is the velocity (m/s) of species i and u_i^0 is the free-settling ('Stokes') velocity of an isolated particle of species i. Critically also, f_i is the hindered settling function of the R-Z model for monodisperse systems that is directly applied to polydisperse systems. It dictates the changes in sedimentation velocity with total particle volume fraction, $\phi = \Sigma\ \phi_i$, where n is an empirical value that is often quoted to be in the range of 4.65–6 [55], depending on conditions such as Reynolds number. In this study, the value of n was taken as 5.1, as determined for spherical particles at low Reynolds numbers by Garside and Al-Dibouni [56], although, given the small total volume fractions, a variance of n within this range would only modify predicted settling rates in the order of 1%.

In addition to the Richardson-Zaki model, data was compared with the Al-Naafa and Selim [16] modified Bachelor settling model [57] in a wider volume fraction range. Bachelor's theory is based on pairwise particle interactions, and has been shown to match well with experimental data in relatively dilute suspensions [16,17]. Linear hindrance coefficients are used to describe the hindering effect. The hindered settling velocity, v_i, of a particle of species (i) in a polydisperse suspension of, N, discrete particles is given by Eq. (8):

$$v_i = u_i^0 (1 + \sum_{j=1}^{N} S_{ij}\phi_j) \tag{8}$$

Here, again, u_i^0 is the Stokes velocity of species i, while ϕ_j is the volume fraction of species j in the mixture. Also, S_{ij} are dimensionless sedimentation coefficients from the study of Batchelor and Wen [15], which are related to the size ratio ($\lambda = d_j/d_i$, or 1.6 and 5 in the 500:800 and 100:500 cases) and the relative density ratio

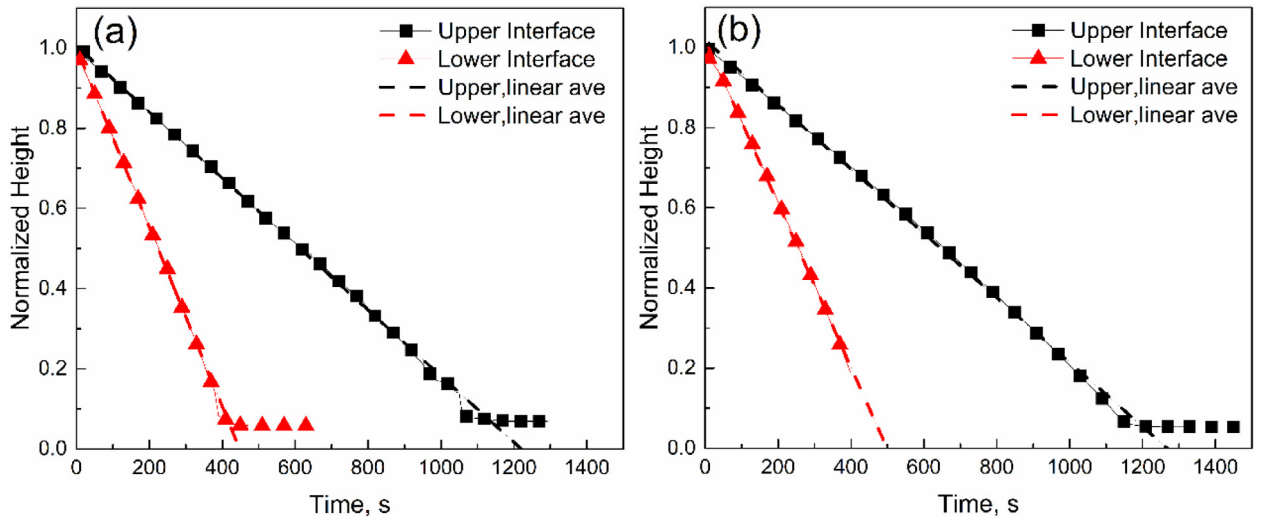

Fig. 6. Normalised sedimentation front versus time data for 500 and 800 nm particle dispersions (at a 1:1 concentration ratio) under a centrifuge speed of 1000 rpm, and total volume fractions of (a) 0.001, and (b) 0.015. Dashed lines represent average interpolated linear settling rates for each species.

($\gamma = (\rho_j - \rho_f)/(\rho_i - \rho_f) = 1$) of the bidisperse system. Thus, the hindered settling velocities of upper and lower interfaces can be obtained. The S_{ij} values used in this study are recorded within the ESM (Eqs. S1-4) following the values set by Batchelor and Wen for the given size ratios [15].

The Stokes terminal velocity can be independently calculated for spherical particles under centrifugal acceleration by Eq. (9):

$$u_i^0 = \frac{d^2(\rho_d - \rho_c)a}{18\mu_c} \tag{9}$$

where d is the disperse phase diameter (m), ρ_d is the dispersed phase density (kg/m^3), and a is the acceleration experienced (m/s^2). Additionally, ρ_c (kg/m^3) and μ_c (Pa.s) are the density and viscosity of the continuous phase, respectively.

When particles of two sizes are settling together, the upflow of displaced fluid is caused by the combined effect of the sedimentation of the larger and smaller particles. In Al-Naafa and Selim's paper [16], the upper zone and lower zone are separated and the sedimentation coefficients are related to each specific species concentration. For the lower zone, two expressions for sedimentation velocities in the combined settling zone were proposed by them, as given in Eq. (10) and Eq. (11), where v is the settling velocity, l and s are the large and small particles, respectively, and the subscript '2′ refers to the subscripts '1′and '2′ refer to the upper and lower zone.

$$v_{l,2} = (1 - \phi_l - \phi_s)^{5.55}[u_l^0(1 - \phi_l) - u_s^0\phi_s] \tag{10}$$

$$v_{s,2} = (1 - \phi_l - \phi_s)^{5.55}[u_s^0(1 - \phi_s) - u_l^0\phi_l] \tag{11}$$

For the upper zone, the lower zone settling velocities $v_{l,2}$ and v_{s2} are used to calculate the volume fraction $\phi_{s,1}$ which can be expressed as given in Eq. (12), where $\phi_{s,2}$ is the initial concentration of the smaller particle species.

$$\phi_{s,1} = \frac{v_{l,2} - v_{s,2}}{v_{l,2} - v_{s,1}}\phi_{s,2} \tag{12}$$

Since the upper zone contains only the slower-settling smaller particles, the settling velocity of upper zone is given more simply as Eq. (13) [16].

$$v_{s,1} = u_s^0(1 - \phi_{s,1})^{6.55} \tag{13}$$

The work of Al-Naafa & Selim [16], who also studied dilute suspensions of nanoparticles (ϕ < 0.03), confirmed the theoretical exponent prediction of 6.55 given by Batchelor [14] and thus is also used in the current model. As the volume concentration in this study is < 0.05, the velocity of the upper zone [19] in dilute suspension can be given as per Eq. (14). Eq.(12) and (14) can then be solved simultaneously for $\phi_{s,1}$ and v_{s1}.

$$v_{s,1} = u_s^0(1 - 6.55\phi_{s,1}) \tag{14}$$

Fig. 7 presents both the upper and lower interface settling rate data for 500:800 particle mixtures with ratios of 1:2, 1:1 and 2:1 (data generated at both 1000 and 2000 rpm are shown). Settling rates are compared to both the Richardson & Zaki power-law model and the Al-Naafa & Selim ('N—S') modified Batchelor model, where the upper interface was predicted using a 500 nm particle size to calculate the initial settling rate (u_1^0), and the lower interface using an 800 nm size (u_2^0). It is noted also that while the lower (faster) settling interface could only be detected for total volume fractions < 0.02, the upper (slower) settling interface was measured for total volume fractions up to 0.05.

In particular for mixing ratios of 1:2 and 1:1, the upper (slower) settling interface is better predicted by the R-Z model, where the N—S model slightly overpredicts sedimentation. The lower (faster) interface settles at rates slightly below those of either theoretical models (inferring enhanced hindered settling) although it is better predicted by the N—S model, up to the instrument limit of detection (consistent with previous work which used the Batchelor model [58]). For the 2:1 ratio case, both models give a similar prediction for the larger particles, while in this case, the smaller particles have a reduced settling rate in comparison to either model (inferring enhanced hindered effects for the upper zone). Both models give overall best predictions for the 1:1 case. Therefore, it is clear then that the relative particle ratios affect sedimentation, for the same total concentration, implying mixture fractions influence the hindered settling behaviour. In addition, the effect of centrifugal force on the accuracy of model predictions is minimal, as there is little difference in correlation between the 1000 and 2000 rpm cases (although the actual settling rates are considerably different) implying that the accelerated fractionation is not considerably affecting results.

Other hydrodynamic or dispersion interactions between particle fractions may also contribute to a modified hindering effect, which is not considered by the model functions. For example, particle wake effects can cause further drag and what is known

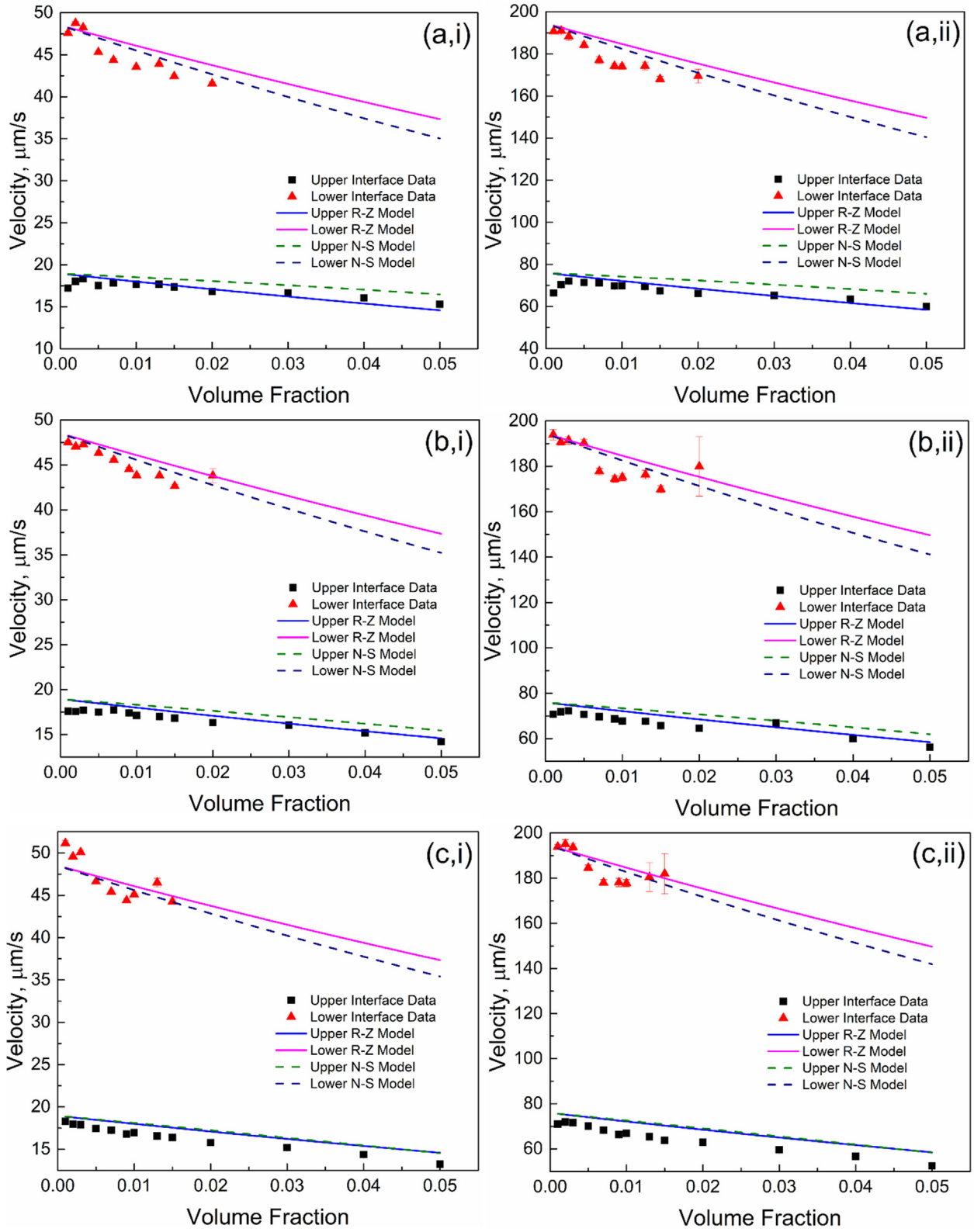

Fig. 7. Comparison of averaged linear settling velocities for 500 and 800 nm mixed particle dispersions at various total volume fractions, to calculated estimations using the Richardson & Zaki ('R-Z') [13] and Al-Naafa & Selim ('N—S') [16] models. Shown is data for relative 500:800 nm particle ratios of (a) 1:2, (b) 1:1, and (c) 2:1, all under centrifuge speeds of (i) 1000 rpm and (ii) 2000 rpm.

as 'drafting-kissing-tumbling' events, but these are generally found for systems with Reynolds number > 1 (e.g., Zaidi *et al.* [43]) whereas Reynolds numbers estimated from terminal velocities in the current study are in the order of 10^{-4}-10^{-3}. Simulations by Yin & Koch [42] explained reduced settling rates in terms of structural anisotropy that occurs in the dispersions, although again,

effects were most evident for larger Reynolds numbers than the studies case. However, we believe they may be more pronounced in bidisperse systems, where the larger particles settle through the smaller fraction. For example, previous simulations of bidisperse colloidal suspensions at low Reynolds number by Abbas *et al.* [58] indicated that particle diffusion and transverse velocities can be significantly modified for each phase, depending on the mixture ratio, leading to variance in settling velocities. Additionally, bidisperse simulations by Koo [59] again for relevant low Reynolds numbers, showed consistently that settling velocities were lower than empirical predictions at low total volume fractions, and varied depending on size ratio.

3.3. Sedimentation of 100 and 500 nm particle mixtures

One potential difference between the 100:500 nm particle mixtures and the 500:800 nm systems, is the increased influence of Brownian motion on the smaller 100 nm species. To illustrate the effect of Brownian motion, the Peclet number [60], which is the ratio of the advective transport and diffusive transport rates, can be calculated using the terminal velocity of particles. For l, the characteristic length (m) of particle, taken as the diameter, v the relative flow velocity, taken as the terminal settling velocity (m/s), and D (m^2/s) the mass diffusion coefficient of the particles in fluid, the Peclet number can be calculated from the Stokes-Einstein equation [61]:

$$Pe = \frac{vl}{D} \tag{15}$$

Peclet number calculations are given Table 1 for both 100 and 500 nm particles at various centrifuge speeds from 1000 to 4000 rpm. In general, Peclet numbers < 0.1 infer diffusion dominated behaviour [62]. Using this threshold, it is clear that in the lower rpm region (below 3000 rpm) the behaviour of 100 nm silica particles is mainly controlled by Brownian motion [63], which may lead to a reduction in the clarity of the upper interface fraction observed through transmission.

The interface transmission profiles for the 100:500 nm particle mixtures are shown within the ESM (Fig. S8) for an overall volume fraction of 0.01 and a 1:1 particle ratio. Indeed, it is evident that for lower rpm (1000 & 2000 rpm) the upper interface is not easily discernible at all. However, for 3000 and 4000 rpm, both particle fractions can be detected with separate interfaces. We believe Brownian diffusion of the 100 nm particles at the lower rpm is significant enough to continue mixing with the larger particle fraction, reducing the separation. Therefore, for the main experiments presented, only data at 4000 rpm was analysed for the 100:500 nm particle systems. A further example of the raw transmission profiles is given in Fig. 8 (for the case of a 1:1 particle ratio and total volume fraction of 0.02).

From the transmission profiles in Fig. 8, there was some other interesting behaviour observed for the upper (100 nm) particle fraction. In particular, there was evidence of an oscillation phenomenon towards the beginning of the sedimentation in the upper transmission area near the meniscus (see annotated box in the figure). We believe that, despite the high 4000 rpm centrifuge, this observed oscillation may be due to Brownian motion of the

Table 1
Peclet numbers for 100 nm and 500 nm silica particles under different centrifugal rotation speeds, using their terminal velocities.

Particle size	1000 rpm	2000 rpm	3000 rpm	4000 rpm
100 nm	0.01	0.04	0.09	0.16
500 nm	0.64	25.68	57.71	102.61

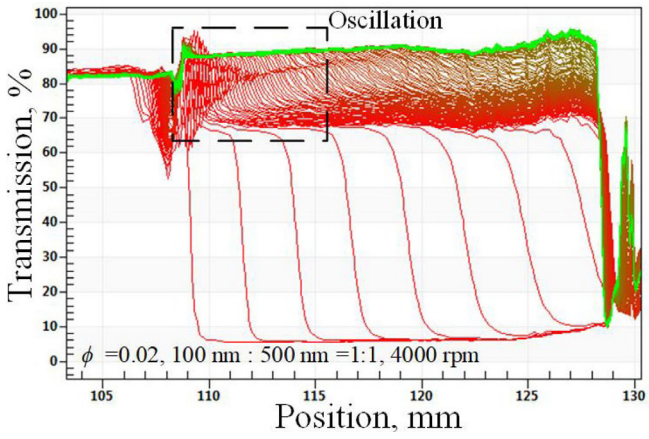

Fig. 8. LUMiSizer® transmission profiles of bidisperse silica suspensions (100 and 500 nm particles) at a volume ratio of 1:1 and total volume fraction of 0.02, under a 4000 rpm centrifuge speed.

100 nm particles still having some effect. In general, there will be some time lag before the smaller 100 nm particles attain their terminal velocity in the high gravity field due to the competing Brownian motion, which makes the initial profiles relatively noisy. In addition, it may indicate some nanoparticle adsorption either to the liquid meniscus itself or to the tube walls. While these were uncoated silica nanoparticles, they may still have a large enough particle contact angle to adsorb to air–water interfaces, although detachment energies should still be low [64]. It also may be a direct optical effect of the meniscus or upper discontinuity in the tube. It is noted that due to the much larger size ratio for the 100:500 nm particle case, the relative transmission of the 100 nm particles is much greater than for the 500 nm particles, making any distinction of the upper particle zone difficult at low total concentrations.

Despite these additional variations, average settling rates from each particle fraction were still successfully measured for a range of particle mixture ratios and total volume fractions. Fig. 9 presents two examples of the particle fraction interface versus time data for the 100:500 nm particle mixtures at different total volume fractions (and a 1:1 relative particle ratio). Fig. S9 within the ESM gives further examples of settling data from other total volume fractions analysed with the same particle ratio. In general, average linear settling rates for both particle fractions were clearly estimated from these figures (shown by the dashed lines) although the interfacial data is noisier for the 100 nm fraction at low total particle levels (likely due to the competing influence of Brownian motion, as discussed).

Using these calculated averages, the settling velocities of the 100:500 nm particle mixtures in different volume fractions are shown in Fig. 10 (i, a-c), again in comparison to estimations from the R-Z power-law model and the N—S modified Batchelor model. Evaluations are similarly made at three different particle mixture ratios (1:2, 1:1 and 2:1 relative ratios). From the results, both models predict the settling rates of both particle species to a greater accuracy than the 500:800 nm systems, likely because of the larger degree of separation in particle settling rates from the wider size ratio and centrifuge speed. The modified Batchelor model does also give some improvement in prediction for the larger (faster settling) particle fraction, especially in the case where there is a greater degree of larger particles in the mixtures, likely due to the separation of the individual particle fractions within the model.

Fig. 10 (ii, a-c) displays further analysis into the interaction between particle species. Specifically, the measured settling velocity of smaller particles was estimated in different sections; being

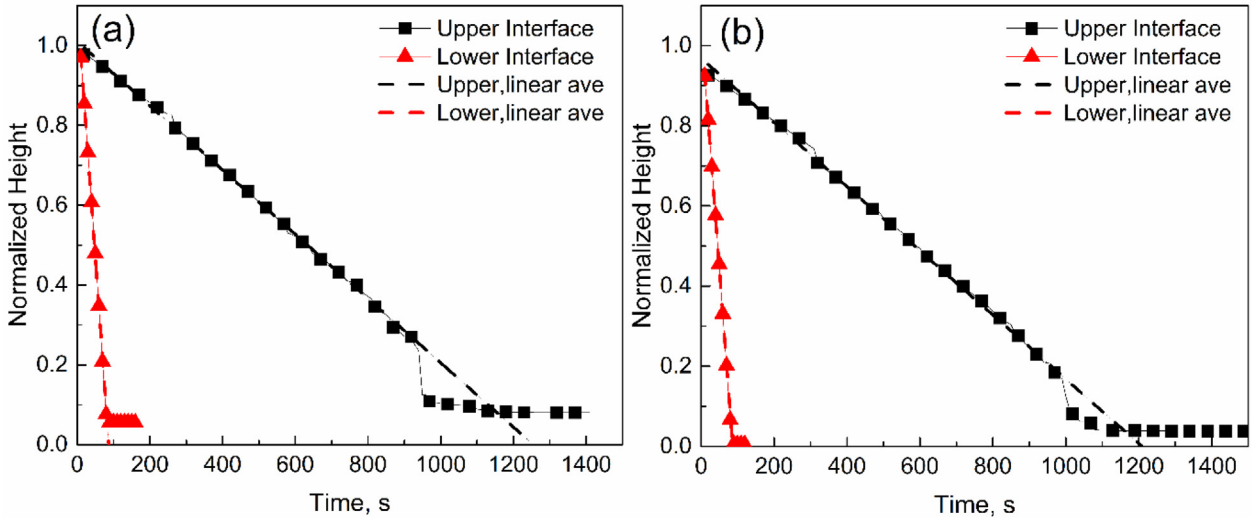

Fig. 9. Normalised sedimentation front versus time data for 100: 500 nm particle dispersions (at a 1:1 concentration ratio) under a centrifuge speed of 4000 rpm, and total volume fractions of (a) 0.015, and (b) 0.03. Dashed lines represent average interpolated linear settling rates for each species.

those before complete sedimentation of the larger 500 nm fraction (black circles) and those afterwards (inverted red triangles) in comparison to the calculated terminal velocity.

It is observed that in all cases, that the initial settling rate of the 100 nm particles is slower than the rate post 500 nm particle deposition, meaning that the 500 nm particles further hindered the sedimentation of the 100 nm fraction. This effect also appears more significant in mixtures with a greater ratio of 100 nm particles, highlighting the impact of the relative concentration of the smaller species again, in which the larger particles sediment through (consistent with the 500:800 case).

The increase in the settling rate post deposition of the 500 nm species may be explained by the reduced overall hindered settling effects from the lower total volume fraction once the 500 nm particles have sedimented (and this relative effect is more significant for cases of higher 500 nm ratios). However, there is also evidence of greater hindering effects for the sedimentation of the smaller species in the initial times when the two fractions are in contact. Again, we believe there is enhanced dispersion anisotropy from the larger particles settling through the smaller fraction, while due to the greater size ratio, backflow effects may be heightened, which have experimentally been determined to influence sedimentation of spheres in Stokes flow regimes where $Re \ll 1$ [65,66]. As an extension, Howard et al. [67] highlighted effects of upflow and zonal banding in simulations of heavy particles in mutually buoyant suspensions subjected to variable shear, all be it for systems at higher concentrations. There is also potential for the 100 nm aggregates to affect sedimentation by increasing the local effective volume fraction of the dispersion in the initial region before they settle out. Lastly, a comment is made regarding the influence of these dispersion effects on non-spherical systems, which may be of more interest industrially. Given that drag is enhanced in non-spherical particle systems [68,69], any hydrodynamic influence of particle phases settling through one another will be heightened, potentially reducing phase separation more than for spherical systems.

4. Conclusions

In this study, centrifugal sedimentation experiments were conducted with bidisperse colloidal silica dispersions in two different size ratios, using an analytical photo centrifuge (LUMiSizer®). Specifically, particle mixtures of 500:800 nm dispersions (mean size ratio of 1.6) and 100:500 nm dispersions (mean size ratio of 5) were investigated at three different volume mixture ratios (1:2, 1:1 and 2:1) to understand the importance of fluid-particle effects from the larger size fraction on the settling of the smaller particles. Results were compared to modified empirical models to predict the influence of total volume fraction on settling rate. For truly dilute suspensions (where the influence of volume fraction is ignored) the LUMiSizer® was able to gain very reproducible size distributions for both monodisperse and bidisperse systems, by integration of the velocity distribution (and using Stokes law to convert to size). Distributions compared very well to estimates from SEM and manufacturer expectations, and in fact, were a lot closer than measurements using dynamic light scattering (DLS) with a Zetasizer®. In particular, results showed that DLS is not very suitable to measure the size distribution of colloidal bidisperse suspensions, where size peaks may overlap.

For sedimentation studies at various total volume fractions, the LUMiSizer® was shown to have an upper concentration limitation where only one interface could be detected by the instrument. For the 500:800 nm mixtures, this volume fraction was ~ 0.015 for most mixtures. However, below this limitation, both particle fractions separated clearly, and average settling rates of each size fraction were able to be analysed. Settling data was compared to the Richardson-Zaki [13] model and the modified Batchelor model of Al-Naafa & Selim [16]. The 500:800 nm particle mixture data, in general, compared well to both models, although the Batchelor model proved more accurate at predicting the lower faster interface rate (of the larger particles) while both models slightly over predicted the upper slower interface (smaller particle fraction). Correlation was also dependent on the mixture ratio, with predictions poorest for systems with higher fractions of smaller particles. It appears that the smaller particle fraction experiences a greater degree of hindrance than modelled, which may be due to dispersion anisotropy or backflow causing enhanced drag from the larger particle fraction, as it settles through the smaller particle zone.

For the case of the 100:500 nm particle mixtures, it was evident that Brownian motion was contributing significantly to the overall movement of the 100 nm particles, which was confirmed with estimation of the Peclet number. Therefore, higher centrifugal rotation rates (of 3000 and 4000 rpm) had to be used to clearly separate the particle fractions. Again, interfacial settling data was compared to the empirical models, where the modified Batchelor model pro-

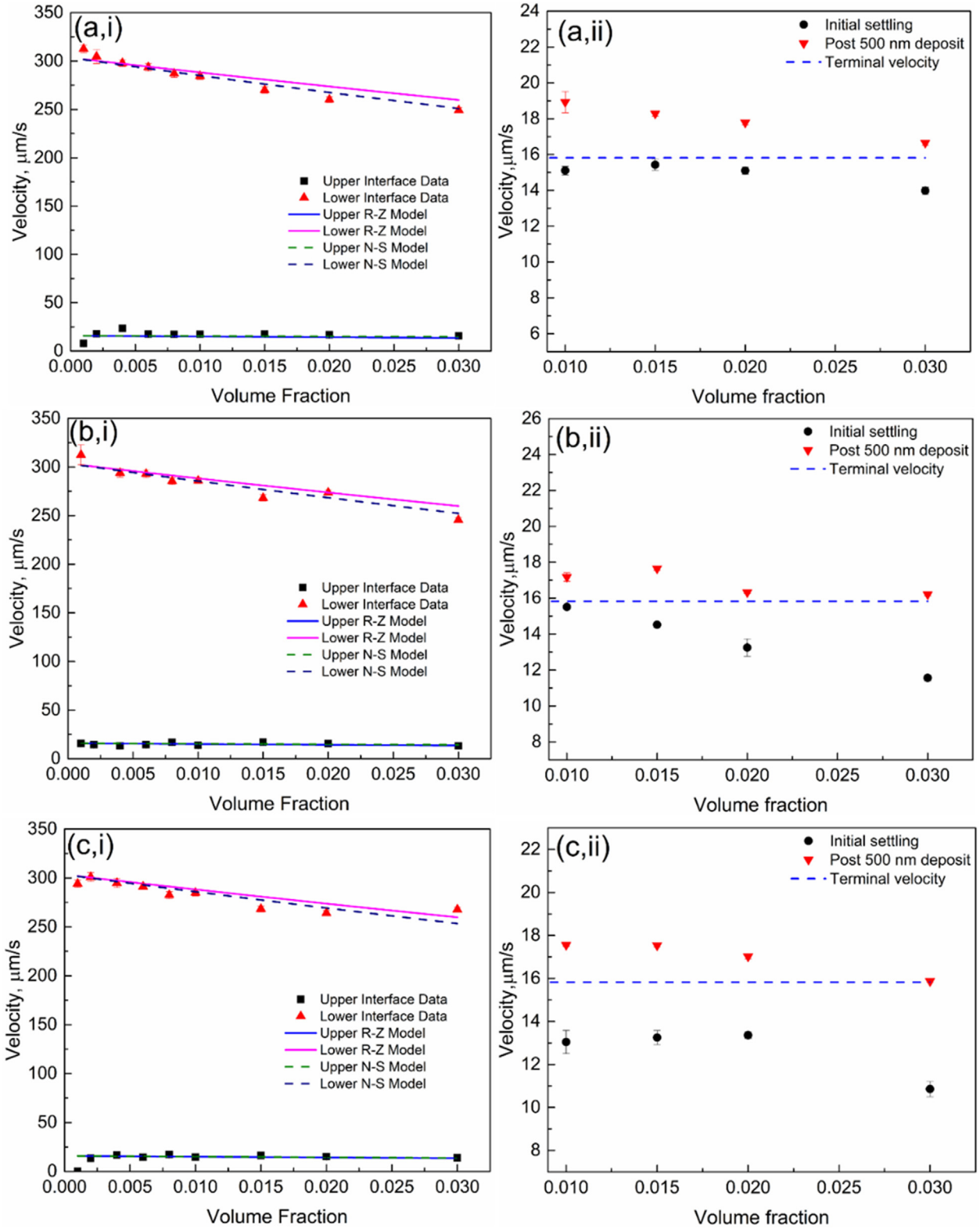

Fig. 10. (i) Comparison of averaged linear settling velocities for 100 and 500 mixed particle dispersions at various total volume fractions, against calculated estimations using the Richardson & Zaki ('R-Z') [13] and Al-Naafa & Selim ('N—S') [16] models. (ii) The analysis of 100 nm particle velocities before and after 500 nm particle fraction has settled. Data is given for particle ratios of (a) 1:2, (b) 1:1, and (c) 2:1.

vided better estimates again for the lower interface (larger particles). In this case, the influence of the larger particle fraction was highlighted by analysing the velocity of the upper (smaller) particle fraction before and after sedimentation of the larger particles. Again, evidence of enhanced drag was evident in the separation of the smaller 100 nm particles, where their initial settling velocity was below their predicted terminal velocity within the initial time window before complete sedimentation of the larger particles.

Once more, these effects were more prevalent for systems with a greater volume fraction of smaller species. Overall, results highlighted the practical advantages and limitations of using analytical photo centrifuges for characterisation of bidisperse sedimentation. It also suggests a more complete model is required to take into account the additional hindrance factors evidenced, and in particular, the influence of particle mixture ratio.

Declaration of Competing Interest

The authors declare that they have no known competing financial interests or personal relationships that could have appeared to influence the work reported in this paper.

Acknowledgements

The authors would like to acknowledge the support of Stuart Micklethwaite and the Leeds Electron Microscopy and Spectroscopy (LEMAS) centre in conduction of the SEM analysis.

Appendix A. Supplementary data

Supplementary data to this article can be found online at https://doi.org/10.1016/j.apt.2023.103950.

References

[1] J. Bloesch, N. Burns, A critical review of sedimentation trap technique, Schweizerische Zeitschrift für Hydrologie 42 (1980) 15–55.
[2] D.B. Siano, Layered sedimentation in suspensions of monodisperse spherical colloidal particles, Journal of Colloid and Interface Science 68 (1979) 111–127.
[3] F. Concha, R. Bürger, A century of research in sedimentation and thickening, KONA powder and particle Journal 20 (2002) 38–70.
[4] K. Marton, J. Balogh, J. Džmura, J. Petráš, Elimination of dust particle sedimentation in industry environment, Journal of Electrostatics 71 (2013) 208–213.
[5] T.N. Hunter, J. Peakall, D. Egarr, D.M. Cowell, S. Freear, A.S. Tonge, L. Horton, H. P. Rice, I. Smith, K. Malone, Concentration profiling of a horizontal sedimentation tank utilising a bespoke acoustic backscatter array and CFD simulations, Chemical Engineering Science 218 (2020).
[6] A.P. Lockwood, J. Peakall, N.J. Warren, G. Randall, M. Barnes, D. Harbottle, T.N. Hunter, Structure and sedimentation characterisation of sheared Mg (OH) 2 suspensions flocculated with anionic polymers, Chemical Engineering Science 231 (2021).
[7] N. Dulova, M. Trapido, Application of Fenton's reaction for food-processing wastewater treatment, Journal of Advanced Oxidation Technologies 14 (2011) 9–16.
[8] P. Bartlett, L.J. Teece, M.A. Faers, Sudden collapse of a colloidal gel, Physical Review E 85 (2012).
[9] S. Vesaratchanon, A. Nikolov, D.T. Wasan, Sedimentation in nano-colloidal dispersions: effects of collective interactions and particle charge, Advances in colloid and interface science 134 (2007) 268–278.
[10] J. Padding, A. Louis, Interplay between hydrodynamic and Brownian fluctuations in sedimenting colloidal suspensions, Physical Review E 77 (2008).
[11] E. Antonopoulou, C.F. Rohmann-Shaw, T.C. Sykes, O.J. Cayre, T.N. Hunter, P.K. Jimack, Numerical and experimental analysis of the sedimentation of spherical colloidal suspensions under centrifugal force, Physics of Fluids 30 (2018).
[12] D.-Q. Cao, E. Iritani, N. Katagiri, Solid-Liquid Separation Properties in Centrifugal Sedimentation of Bidisperse Colloidal Suspension, Journal of Chemical Engineering of Japan 48 (2015) 556–563.
[13] J. Richardson, W. Zaki, The sedimentation of a suspension of uniform spheres under conditions of viscous flow, Chemical Engineering Science 3 (1954) 65–73.
[14] G. Batchelor, Sedimentation in a dilute dispersion of spheres, Journal of fluid mechanics 52 (1972) 245–268.
[15] G. Batchelor, C.-S. Wen, Sedimentation in a dilute polydisperse system of interacting spheres. Part 2. Numerical results, Journal of Fluid Mechanics 124 (1982) 495–528.
[16] M. Al-Naafa, M.S. Selim, Sedimentation of monodisperse and bidisperse hard-sphere colloidal suspensions, AIChE Journal 38 (1992) 1618–1630.
[17] R. Davis, K. Birdsell, Hindered settling of semidilute monodisperse and polydisperse suspensions, AIChE Journal 34 (1988) 123–129.
[18] C. Reed, J.L. Anderson, Hindered settling of a suspension at low Reynolds number, AIChE Journal 26 (1980) 816–827.
[19] J.F. Brady, L.J. Durlofsky, The sedimentation rate of disordered suspensions, The Physics of fluids 31 (1988) 717–727.
[20] G.J. Kynch, A theory of sedimentation, Transactions of the Faraday society 48 (1952) 166–176.
[21] K. Davis, W.B. Russel, An asymptotic description of transient settling and ultrafiltration of colloidal dispersions, Physics of Fluids A, Fluid Dynamics 1 (1989) 82–100.
[22] B.B. van Deventer, S.P. Usher, A. Kumar, M. Rudman, P.J. Scales, Aggregate densification and batch settling, Chemical Engineering Journal 171 (2011) 141–151.
[23] R. Dorrell, A.J. Hogg, Sedimentation of bidisperse suspensions, International Journal of Multiphase Flow 36 (2010) 481–490.
[24] J.t. RICHARDSON, Sedimentation and fluidisation: Part I, Transactions of the Institution of Chemical Engineers 32 (1954) 35–53.
[25] R.H. Davis, H. Gecol, Hindered settling function with no empirical parameters for polydisperse suspensions, AIChE journal 40 (1994) 570–575.
[26] S. Mirza, J. Richardson, Sedimentation of suspensions of particles of two or more sizes, Chemical Engineering Science 34 (1979) 447–454.
[27] P. Krishnamoorthy, Sedimentation model and analysis for differential settling of two-particle-size suspensions in the Stokes region, International journal of sediment Research 25 (2010) 119–133.
[28] M.K. Cheung, R.L. Powell, M.J. McCarthy, Sedimentation of noncolloidal bidisperse suspensions, AIChE journal 42 (1996) 271–276.
[29] Y. Zimmels, Theory of hindered sedimentation of polydisperse mixtures, AIChE journal 29 (1983) 669–676.
[30] J. Chong, E. Christiansen, A. Baer, Rheology of concentrated suspensions, Journal of applied polymer science 15 (1971) 2007–2021.
[31] J. Shiels, D. Harbottle, T.N. Hunter, Synthesis and physical property characterisation of spheroidal and cuboidal nuclear waste simulant dispersions, Materials 11 (2018) 1235.
[32] C. Chu, D. Lee, Experimental analysis of centrifugal dewatering process of polyelectrolyte flocculated waste activated sludge, Water Research 35 (2001) 2377–2384.
[33] S.P. Usher, L.J. Studer, R.C. Wall, P.J. Scales, Characterisation of dewaterability from equilibrium and transient centrifugation test data, Chemical Engineering Science 93 (2013) 277–291.
[34] V. Sviatskii, A. Repko, D. Janačova, Z. Ivandič, O. Perminova, Y. Nikitin, Regeneration of a fibrous sorbent based on a centrifugal process for environmental geology of oil and groundwater degradation, Acta Montanistica Slovaca (2016).
[35] R. Mao, J. Tang, B. Swanson, Water holding capacity and microstructure of gellan gels, Carbohydrate polymers 46 (2001) 365–371.
[36] X. Meng, Y. Zhu, Y. Chen, Y. Lu, Y. Xu, J. Cheng, Conditional siphon priming for multi-step assays on centrifugal microfluidic platforms, Sensors and Actuators B: Chemical 242 (2017) 710–717.
[37] T. Sobisch, D. Lerche, Separation behaviour of particles in biopolymer solutions in dependence on centrifugal acceleration: Investigation of slow structuring processes in formulations, Colloids and Surfaces A: Physicochemical and Engineering Aspects 536 (2018) 74–81.
[38] D. Lerche, Comprehensive characterization of nano-and microparticles by in-situ visualization of particle movement using advanced sedimentation techniques, KONA Powder and Particle Journal 36 (2019) 156–186.
[39] H.-T. Chiu, C.-Y. Chang, T.-Y. Chiang, M.-T. Kuo, Y.-H. Wang, Using analytical centrifugation to characterize the dispersibility and particle size distributions of organic/inorganic composite coatings, Journal of Polymer Research 18 (2011) 1587–1596.
[40] A. Braun, O. Couteau, K. Franks, V. Kestens, G. Roebben, A. Lamberty, T. Linsinger, Validation of dynamic light scattering and centrifugal liquid sedimentation methods for nanoparticle characterisation, Advanced Powder Technology 22 (2011) 766–770.
[41] X. Xu, P.M. Biesheuvel, H. Cölfen, E. Spruijt, Layering of bidisperse charged nanoparticles in sedimentation, Soft matter 16 (2020) 4718–4722.
[42] X. Yin, D.L. Koch, Hindered settling velocity and microstructure in suspensions of solid spheres with moderate Reynolds numbers, Physics of Fluids 19 (2007).
[43] A.A. Zaidi, T. Tsuji, T. Tanaka, Direct numerical simulations of inertial settling of non-Brownian particles, Korean Journal of Chemical Engineering 32 (2015) 617–628.
[44] S. Dash, T. Lee, Two spheres sedimentation dynamics in a viscous liquid column, Computers & Fluids 123 (2015) 218–234.
[45] J. Hu, Z. Guo, Effect of interaction between a particle cluster and a single particle on particle motion and distribution during sedimentation: A numerical study, Physics of Fluids 31 (2019).
[46] E.D. Hyde, A. Seyfaee, F. Neville, R. Moreno-Atanasio, Colloidal silica particle synthesis and future industrial manufacturing pathways: a review, Industrial & Engineering Chemistry Research 55 (2016) 8891–8913.
[47] W. Hergert, T. Wriedt, The Mie theory: basics and applications, Springer, 2012.
[48] T. Detloff, T. Sobisch, D. Lerche, Particle size distribution by space or time dependent extinction profiles obtained by analytical centrifugation, concentrated systems, Powder Technology 174 (2007) 50–55.
[49] Y. San Chan, M.M. Don, Biosynthesis and structural characterization of Ag nanoparticles from white rot fungi, Materials Science and Engineering: C 33 (2013) 282–288.
[50] W. Anderson, D. Kozak, V.A. Coleman, Å.K. Jämting, M. Trau, A comparative study of submicron particle sizing platforms: accuracy, precision and resolution analysis of polydisperse particle size distributions, Journal of colloid and interface science 405 (2013) 322–330.
[51] J.S. Behra, J. Mattsson, O.J. Cayre, E. Robles, H. Tang, T.N. Hunter, Characterization of Sodium Carboxymethyl Cellulose (Na CMC) aqueous

solutions to support complex product formulation – a rheology and light scattering study, Acs Applied Polymer Materials (2019).
[52] W. Anderson, D. Kozak, V.A. Coleman, K. J?Mting, M. Trau, A comparative study of submicron particle sizing platforms: Accuracy, precision and resolution analysis of polydisperse particle size distributions, J Colloid Interface 405 (2013) 322–330.
[53] G.A. Schumacher, T.G. van de Ven, Brownian motion of charged colloidal particles surrounded by electric double layers, Faraday Discussions of the Chemical Society 83 (1987) 75–85.
[54] C. Ullmann, F. Babick, R. Koeber, M. Stintz, Performance of analytical centrifugation for the particle size analysis of real-world materials, Powder Technology 319 (2017) 261–270.
[55] M. Johnson, J. Peakall, M. Fairweather, S. Biggs, D. Harbottle, T.N. Hunter, Characterization of multiple hindered settling regimes in aggregated mineral suspensions, Industrial & Engineering Chemistry Research 55 (2016) 9983–9993.
[56] J. Garside, M.R. Al-Dibouni, Velocity-voidage relationships for fluidization and sedimentation in solid-liquid systems, Industrial & engineering chemistry process design and development 16 (1977) 206–214.
[57] G. Batchelor, Sedimentation in a dilute polydisperse system of interacting spheres. Part 1. General theory, Journal of Fluid Mechanics 119 (1982) 379–408.
[58] M. Abbas, E. Climent, O. Simonin, M.R. Maxey, Dynamics of bidisperse suspensions under Stokes flows: Linear shear flow and sedimentation, Physics of Fluids 18 (2006).
[59] S. Koo, Sedimentation velocity of bidisperse suspensions, Journal of Industrial and Engineering Chemistry 14 (2008) 679–686.
[60] W. Cui, Z. Shen, J. Yang, S. Wu, Rotation and migration of nanoparticles for heat transfer augmentation in nanofluids by molecular dynamics simulation, Case Studies in Thermal, Engineering 6 (2015) 182–193.
[61] K.A. Dill, S. Bromberg, D. Stigter, Molecular driving forces: statistical thermodynamics in biology, chemistry, physics, and nanoscience, Garland Science, 2010.
[62] C.A. Solari, K. Drescher, S. Ganguly, J.O. Kessler, R.E. Michod, R.E. Goldstein, Flagellar phenotypic plasticity in volvocalean algae correlates with Péclet number, Journal of the Royal Society Interface 8 (2011) 1409–1417.
[63] H. Chung, R. Hogg, The effect of Brownian motion on particle size analysis by sedimentation, Powder technology 41 (1985) 211–216.
[64] T.N. Hunter, G.J. Jameson, E.J. Wanless, Determination of contact angles of nanosized silica particles by multi-angle single-wavelength ellipsometry, Australian Journal of Chemistry 60 (2007) 651–655.
[65] C.C. Reed, J.L. Anderson, Hindered settling of a suspension at low Reynolds number, AIChE Journal 26 (1980).
[66] A. Ambari, B. Gauthier-Manuel, E. Guyon, Backflow effect in model sedimentation experiments, Physics of Fluids A, Fluid Dynamics 5 (1998) 2061–2063.
[67] A.A. Howard, M.R. Maxey, Y. Kyongmin, Settling of heavy particles in concentrated suspensions of neutrally buoyant particles under uniform shear, Fluid Dynamics Research 50 (2018) 041401-.
[68] H. Yaghoobi, M. Torabi, Analytical solution for settling of non-spherical particles in incompressible Newtonian media, Powder Technology 221 (2012) 453–463.
[69] N. Paul, S. Biggs, J. Shiels, R.B. Hammond, M. Edmondson, L. Maxwell, D. Harbottle, T.N. Hunter, Influence of shape and surface charge on the sedimentation of spheroidal, cubic and rectangular cuboid particles, Powder Technology 322 (2017) 75–83.